3D STRESS AND STRAIN FIELDS AROUND NOTCH AND CRACK TIPS

Rafael Cesar de Oliveira Góes, cesarafael@gmail.com
Jaime Tupiassú Pinho de Castro, jtcastro@puc-rio.br
Luiz Fernando Martha, lfm@tecgraf.puc-rio.br
Marco Antonio Meggiolaro, meggi@puc-rio.br
Pontifical Catholic University of Rio de Janeiro, Rua Marquês de São Vicente 225 – Gávea, Rio de Janeiro, RJ, 22451-900, Brazil

Abstract. *Notches and cracks are usually treated as two-dimensional problems using solutions from plane elasticity to evaluate highly localized stress/strain concentration effects around their tips, which are also associated to high stress gradients that cause three-dimensional fields around those tips that can severely restrict local Poisson-induced transversal strains. Fatigue crack initiation and growth, plastic zone sizes and shapes, and localized constraint effects are typical problems affected by such 3D effects, which may lead to non-conservative damage and life predictions if neglected. To quantify how important they can be, first finite element techniques are used to simulate thickness and notch tip radius effects in the fields around such tips, and to evaluate their importance from the structural design point of view. Then, versatile sub-modeling techniques are used to study similar effects along the fronts of short and long cracks. Finally, a stepwise remeshing routine is used to show how an initially straight crack must slightly curve its front during its propagation by fatigue, due to the unavoidable 3D effects that always surround real crack tips.*

Keywords*: 3D notch and crack tip fields, 3D stress concentration, fatigue crack front curvature, stress gradient effects*

1. INTRODUCTION

For design purposes, the maximum stresses σ_0 that act at notch tips are usually calculated by using a linear elastic (LE) stress concentration factor (SCF) K_t to multiply the nominal stress σ_n that would act there if the notch had no effect on the stress and strain fields that surround it:

$$\sigma_0 = K_t \cdot \sigma_n \tag{1}$$

Circular and elliptical notches were studied by Kirsch and Inglis, and since then a few analytical and many numerical and experimental SCF have been obtained for other notch geometries (Peterson 2008, Savin 1968), but most model the notches by their 2D approximations, assuming plane stress (*pl-σ*), plane strain (*pl-ε*), or axisymmetric conditions. Creager and Paris (1967) estimated SCF from the stress intensity factor (SIF) of a similar crack, but most SIF also assume plane geometries (Tada et al., 2000). However, 2D models of notched components have limitations, even in simple cases like a notched plate loaded by a uniform nominal stress. Far from the notch tip, its material works under *pl-σ*, but the stress/strain fields that surround the tip are in fact 3D, due to the Poisson restriction induced by the gradients that act there. A transversal constraint factor T_z can be defined to quantify this restriction at any point by

$$T_z = \frac{\sigma_z}{\sigma_x + \sigma_y} = \begin{cases} 0, & pl-\sigma \\ \nu, & pl-\varepsilon \end{cases} \tag{2}$$

Since very few analytical solutions are available for 3D fields around notches (Youngdahl & Sternberg 1966), numerical tools are needed to study most 3D SCF problems. Using finite element (FE) to model many notches, Yu et al. (2008) investigated 3D LE fields on tensioned plates, coming to conclusions summarized as follows. SCF along 3D notch tips depend on their shape and thickness-to-tip-radius ratio B/ρ. Although the stresses along the notch front σ_{y0} may vary significantly, the $\sigma_y(x,z')/\sigma_{y0}(z')$ stress ratio distributions ahead of the notch tips at any given z' plane are almost z-independent. Particularly, the $\sigma_{ymp}(x)/\sigma_{y0mp}$ ratio along the notched plate mid-plane $z = 0$ is almost insensitive to the plate thickness B and to the notch shape up to $x/\rho \cong 0.75$, and can be approximated by its 2D solution. Moreover, the 3D affected zone is almost notch shape independent for notches with $a/\rho \geq 1$, and it is limited to a distance of about $3B/8$ from the notch tip. The transversal constraint along the notch tip T_{z0} is maximal at the notch mid-plane and decreases to zero close to the plate free surface. The through-thickness variation of $T_{z0}(z)/T_{z0mp}$ is also nearly independent of the notch shape, and the constraint level decays with the distance from the notch tip. Unlike cracks, notches have finite tip radii and cannot provide enough constraint to reach limit *pl-ε* conditions along the notch fronts. Instead of single SCF $K_t = \sigma_{max}/\sigma_n = \varepsilon_{max}/\varepsilon_n$ used in 2D analyses, independent $K_\sigma = \sigma_{max}/\sigma_n$ and $K_\varepsilon = \varepsilon_{max}/\varepsilon_n$ stress and strain concentration factors should be used to analyze 3D notch problems. The constraint gradient $T_{zmp}(x)/T_{z0mp}$ along the x-direction at the mid-plane ($z = 0$) of notched plates is independent of the notch configuration and tip radius, and can be well fitted by

$$T_{zmp}(x)/T_{z0mp} = 1 - 4.35\left[(1+0.686\,x/B)^{-2} - (1+0.686\,x/B)^{-4}\right] \tag{3}$$

3D crack solutions are scarce as well. Bazant & Estenssoro (1979) related the stress field singularity at the free surface with angle β with which the crack intersects it. For a pure mode I crack, they showed that for $\beta = \pi/2$, K_I must

be zero at the free surface. For the crack to achieve a $r^{-1/2}$ singularity, the $\beta \neq \pi/2$ value solely depends on ν. Nakamura & Parks (1990) studied 3D LE fields around ideally straight crack fronts in thick plates within the SIF-dominated zone, modeling that region as a disk of radius R centered at the tip, assuming the crack size a long compared to the cracked plate thickness ($a >> B$). The disk boundary ($r = R$) was loaded by the displacement field generated by the 2D SIF K_I and K_{II} applied on the plate, the so called Boundary Layer (BL) model. Strong 3D effects were observed within a distance $r = B/2$ from the crack tip, with a 3D-2D transition occurring within $B/2 < r < 3B/2$. The SIF was shown to significantly vary along the crack front when compared with 2D predictions. Albeit ingenious, BL models have limitations. They assume cracks much longer than the thickness, thus do not model well small cracks, with size $a \cong B$ or smaller, an important problem for fatigue predictions. In addition, the cracked plate stress field is obtained assuming that the plate is far-field loaded by the stresses induced by the SIF applied on it. Hence, all K-field assumptions are incorporated by BL models. For instance, K-description for the (assumed LE) stress fields in cracked components is strictly valid only very close to the crack tips, exactly where plasticity-induced perturbations tend to spoil it. Such assumptions also fail to describe the situation where the 3D affected zone surpasses the K-dominated region. Moreover, since K-fields do not reproduce the nominal stresses far from the crack tips, non-negligible effects induced by high σ_n cannot be accounted for by them. Furthermore, ideally straight cracks are just a convenient mathematical trick, as tests show that they propagate with curved fronts, a phenomenon known as crack tunneling. Extensive research on this phenomenon shows that the curved front shape in a through-cracked plate can present a tunneling depth (a_{max} - a_{surf}) up to 0.05 B. This slight curvature is shown to bring considerable impact on SIF calculations along the crack front.

This work first revisits the literature on 3D LE notch analysis and discusses the importance of 3D effects on notch design issues. Then it uses powerful sub-modeling techniques, which avoid the K-field domination and long crack hypothesis limitations, to simulate 3D SIF distributions for large single edge cracked plates with several B/a ratios, and to evaluate their influence on the K_I distribution. Finally, it simulates the 3D growth of an initially straight front crack with initial length a_0, assuming it can be described by the classical Paris rule, to evaluate how the crack front shape and the K_I distribution change as the crack grows.

2. 3D EFFECTS ON STRESS FIELDS AROUND NOTCH TIPS

To evaluate notch-induced 3D stress concentration effects, several Elliptical Holes (EH) and Semi-Elliptical (SE) notches with semi-axes a and b in large tensioned plates of width W and height H were simulated in ABAQUS, using $W/a = H/a = 60$ to avoid boundary effects within *1%* error. To check similar previously published results, $E = 200GPa$ and $\nu = 0.33$ are used, although $\nu = 0.29$ would better match the chosen modulus, a typical value for steels. The models were built with symmetry with respect to the xy plane at the plate mid-thickness and to the xz plane. The EH models received additional symmetry with respect to the yz plane. The uniform load is applied as a uniform tensile stress on the superior plate face $y = H$. The notch tip region is described by structured meshes with a maximum element size of 0.1ρ at the notch tip, where $\rho = b^2/a$ is the notch tip radius. The dimensions of the analyzed notches are listed in Table 1.

Table 1: Elliptical and semi-elliptical notch parameters analyzed in the present FE models.

notch	b/a	ρ/a	B/ρ
elliptical	1	1	0.1, 0.2, 0.4, 0.6, 1, 1.5, 2, 3, 4, 6, 8, 10, 20
	0.5	0.25	0.4, 0.8, 2, 2.8, 4, 6, 8, 12, 16, 32, 48
	0.2	0.04	3, 6, 10, 15, 20, 30, 50, 75, 100
	0.1	0.01	0.4, 0.6, 1, 2, 4, 6, 10, 20, 40, 60, 100
semi-elliptical	1	1	0.2, 0.3, 0.5, 0.7, 1, 2, 3, 5, 7, 10, 20, 30
	0.5	0.25	0.16, 0.24, 0.4, 0.8, 2, 4, 8, 12, 16
	0.2	0.04	0.5, 1, 3, 10, 20, 30
	0.1	0.01	0.6, 6, 10, 20, 40, 60, 100, 200, 400

Figure 1 shows K_σ/K_t and K_ε/K_t distributions along the notch tips of EH with $b/a = 0.5$ and $\rho/a = 0.25$. $K_\sigma \neq K_\varepsilon$, and their maxima occur close to the surface of thick plates (with $B >> \rho$), whereas for thinner plates they occur at the plate center. K_σ/K_t ratios depend on B/ρ, see Fig. 2. In relatively blunt notches (with low B/ρ ratios), σ_{max} and ε_{max} occur at the middle plane of the plate, and in sharper notches they dislocate towards the plate free surfaces (located at $z/B = 0.5$), in a slightly decoupled way. K_σ and K_ε can differ up to 15% in such plates. The maximum SCF at the notch tip $K_{\sigma max}$ can be up to about 8% higher than the 2D SCF K_t, a non-negligible difference. Hence K_t measured as usual at free surfaces may underestimate σ_{max} at notch tips, and 3D effects on stress/strain fields along notch tips may indeed be relevant for some applications. Maxima stress and strain points indicate preferred locations for crack initiation, whereas the stress gradients ahead of such critical points affect how a short crack propagates from them. If cracks prefer to start at maxima stress or strain points, as assumed in most damage models, they should do so at the center of thinner notched plates ($z/B = 0$) and closer to the free surfaces ($z/B = 0.5$) of the thicker ones, but the growth of such initially small surface cracks is strongly dependent on the stress gradient around the notch tip, as discussed elsewhere (Castro et al. 2112). Since the studied notches have much stronger stress gradients in the x than in the z-direction, the short crack driving force de-

crease is sharper ahead than along the notch tip direction. Therefore, cracks initiated at notch tips should prefer to advance first along them trying to become a passing crack, then along the *x*-direction, inwards the specimen. However, although reasonable, such speculations certainly need further investigation, see Góes et al. (2013) for further details.

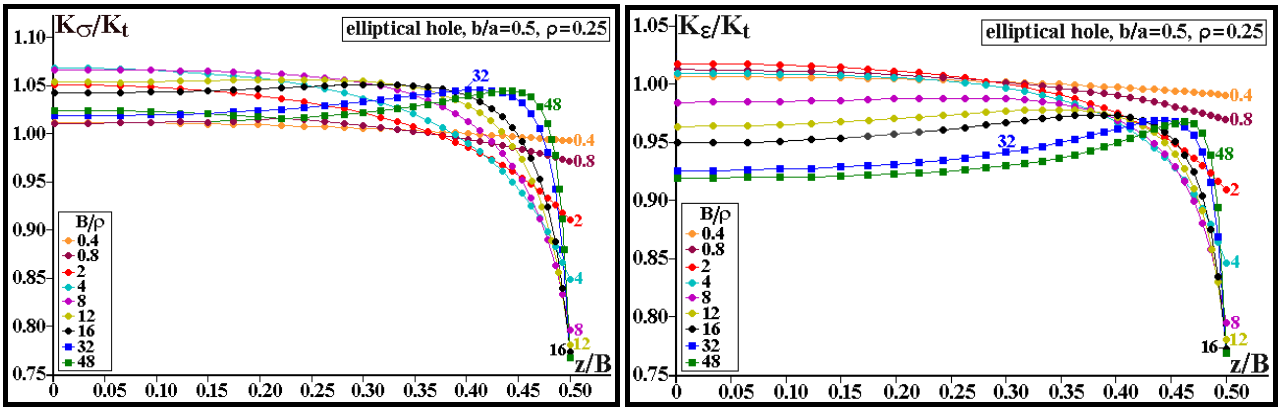

Fig. 1: $K_\sigma/K_t\sigma_n$ and $K_\varepsilon/K_t\varepsilon_n$ distributions along the notch front, for an elliptical hole with $b/a = 0.5$ and $\rho/a = 0.25$.

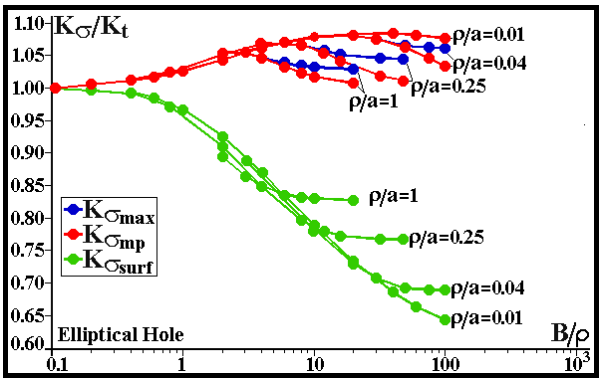

Fig. 2: Variation of $K_{\sigma max}/K_t$, $K_{\sigma mp}/K_t$, and $K_{\sigma surf}/K_t$ with the thickness to notch tip radius ratio B/ρ for elliptical holes.

3. FE MODELS FOR CRACKS AT THE BORDER OF LARGE PLATES

The influence of the thickness-to-crack-size B/a ratio on the crack tip fields of large edge cracked plates under uniaxial loads was evaluated through several LE FE 3D analyses, using sub-modeling techniques to take advantage that most of the plate is expected to respond in *pl*-σ, with 3D stress state limited to the proximities of the crack tip. A large global model for the plate was built using plane elements, with overall dimensions $W_{global}/a = H_{global}/a = 1000$, while several 3D sub-models of the region surrounding the crack were built with B/a ratios varying from 0.1 to 100. In-plane displacement fields (u_x,u_y) from the global model solution were applied to every node of the sub-models boundary surfaces, while their out-of-plane displacements u_z were left free. To maintain kinematic compatibility between global and local solutions, the sub-model dimensions W_{sub}/a, and H_{sub}/a must be chosen so that $T_z \rightarrow 0$ within the sub-model limits. Since the size of the 3D affected zone for an arbitrary B/a value was not known beforehand, the sub-models were built with both W_{sub}/a and $H_{sub}/a > 5B/a$. The results presented following show that such limits were adequately chosen.

Besides numerically efficient, this procedure has some non-negligible advantages over the BL approach. Its crack tip fields are calculated considering all the load characteristics, since they are not restricted by SIF-based hypotheses. It recognizes e.g. nominal stress effects far from the crack tip, which are ignored when *K*-conditions are assumed valid. It also allows analyses of relatively shallow cracks with high B/a ratios. For fatigue life estimations the behavior of such cracks is much more important than the behavior of long cracks. The sub-models were built assuming symmetry with respect to *xy* and *xz* crack planes, using 15 elements along their thickness (the *z*-direction) with sizes varying in geometric progression from the middle-plane (coarser) to the free surface (finer), with a progression ratio $q = 1.3$. The circumferential direction is divided into 24 elements. In the radial direction, the elements are built with size $0.003 \cdot B$ at the very crack tip, coarsening in geometric progression with ratio $q = 1.15$. This refinement is enough to guarantee convergence.

A 2D solution can model this plate far field conditions because it is possible to establish 3 distinct domains for its (LE) stress/strain fields: (i) very far from the crack tip the crack is irrelevant, thus if the plate is large enough this domain works under constant nominal plane stress field conditions, which may be used to model it and its contour conditions; (ii) in the intermediate domain around the crack tip but not within its dominance zone, the crack affects the fields but they remain 2D, since there is no restriction to force them to vary along the *z* direction; (iii) close to the crack tip within its dominance zone such a restriction exists and 3D effects are clearly present, hence the stresses and strains vary along *z*. The intent here is to investigate how such restriction affects short cracks. 3D FE are strictly needed only in this

3rd zone, but it is not possible to precisely model its size prior to its simulation. Even so, sub-modeling allows the 3D model frontier to be reduced and located somewhere within the 2nd domain without the need to assume a (questionable, to say the least) *K*-dominance there, recognizing the nominal stress effects that are not accounted for by the SIF fields and significantly saving computational effort at the same time. Therefore, the simulation results obtained from the sub-models can furnish more information than would be possible to get from assuming a *K*-field around the crack tip.

Figure 3 shows how normalized SIF distributions along idealized straight crack fronts $K_I/K_{I,2D}$ deviate from standard 2D solutions, for a wide range of B/a values including short and long cracks. For long cracks with small B/a, the K_I distribution along the crack front gets closer to standard SIF-dominated far field conditions as expected, but shallow cracks behave differently. Their SIF distribution tends to the 2D solution along most of the crack front, but it shows a peak close to the plate free surface, which does not appear for the long cracks. This difference may affect how they grow by fatigue, thus should not be neglected. Note that "long cracks" mean "cracks large in comparison to the plate thickness B", not to the plate width W. The analysis of very deep cracks, those with large a/W ratios, must include the influence of the back face plane on the LE fields ahead of the crack tip, a problem considered beyond the scope of this work.

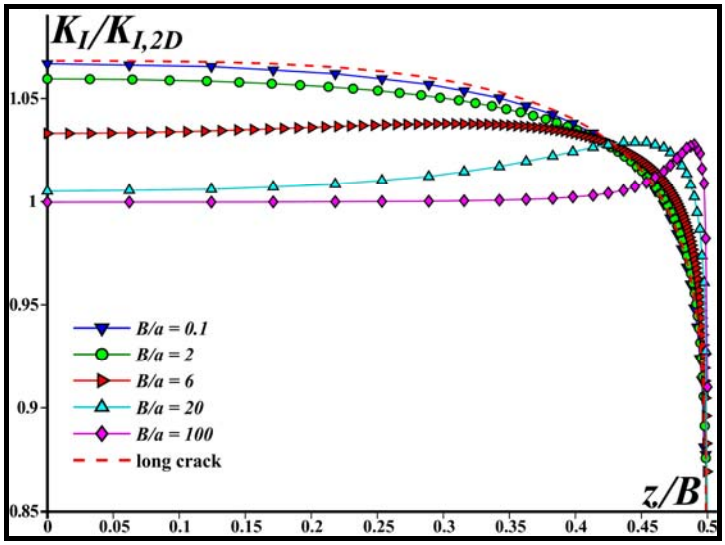

Figure 3: $K_I/K_{I,2D}$ distribution along the front of short and long cracks.

Figure 3 also shows that the SIF drops near the free surface ($z/B = 0.5$). As the crack front is assumed straight and perpendicular to it in such 3D analyses, K_I should be null at that surface, as mentioned above, but such a limit could not be achieved with any reasonable mesh refinement. Anyway, its importance is to force real cracks to slightly curve their fronts during their propagation, as studied next. Figure 4 shows how the ratios $K_{Imax}/K_{I,2D}$ and $K_{Imp}/K_{I,2D}$ vary with B/a, and compares them with the long crack SIF-dominated limit solution from She & Guo (2007). The maxima SIF tend to the long crack solution for cracks with very low B/a, and the middle plate SIFs K_{Imp} tend to the limit 2D solution $K_{I,2D}$ as B/a becomes large and the cracks get shorter. Moreover, the separation of the $K_{Imax}/K_{I,2D}$ curve from the $K_{Imp}/K_{I,2D}$ curve of the short cracks shows that their K_{Imax} value is higher than the reference $K_{I,2D}$ value, about 3% higher for the Poisson coefficient $\nu = 0.3$ used in these numerical simulations, see Góes et al. (2013) for details.

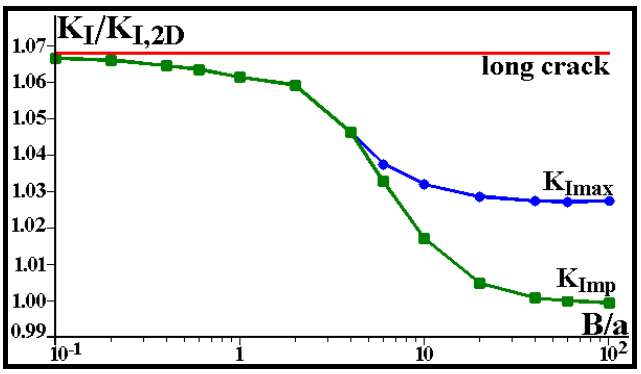

Figure 4: $K_{Imax}/K_{I,2D}$ and $K_{Imp}/K_{I,2D}$ variation with the crack size in large plates.

4. GROWTH OF EDGE CRACKS WITH INITIALLY STRAIGHT FRONTS IN LARGE PLATES

FRANC3D was used to simulate the growth of large and small edge cracks with an initially straight front in large plates, assuming LEFM conditions. Since the solution of LE problems is unique and proportional to the imposed load P,

the calculated SIF K_{cal} along the crack front can be interpreted as a shape function, hence $K_{max} = P \cdot K_{cal}$, $K_{min} = P \cdot R \cdot K_{cal}$, $R = K_{min}/K_{max}$, and $\Delta K = K_{max} - K_{min}$. Without loss of generality, the analyses developed here considered $R = 0$ and $P = 1$, thus in the propagation cases described below $\Delta K = K_{max} = K_{cal}$. Moreover, it is assumed that the local crack advance at any specific point of the crack front follows Paris' fatigue crack growth (FCG) rule. Since the material is assumed isotropic and homogeneous, its FCG behavior along the crack front is also assumed as so, and to depend only on the local crack driving force ΔK, since K_{max}, the other FCG driving force, is fixed. From the K_{cal} values at the crack front nodes in any given step, a crack growth vector $\overrightarrow{\delta a}$ is obtained by a local increment Δa multiplied by a unitary vector $\vec{p}$ in the local crack growth direction, which must be parallel to the crack plane (*xz* in this work notation) and normal to the crack front at each point, as the model is symmetric with respect to the *xz* plane. Since FCG increments are assumed to follow Paris' rule, they can be described for any given node *i* at every *j*-th growth step by

$$\Delta a_{ji} = \Delta a_{jmean} \left(\Delta K_{ji} / \Delta K_{jmean} \right)^n \tag{4}$$

The SIF distribution along the crack front $K(z)$ based on such (reasonable) hypotheses, and the ratios between the SIF increments at each crack front node and the mean SIF increment at each load step, $\Delta K_{ji}/\Delta K_{jmean}$, are all a function of $a_i(z)$, the crack length at each node in that given step. Hence, Δa_{jmean} is an arbitrary analysis parameter, dissociated from the number of load cycles. The crack length at the plate free surface, a_{surf}, is adopted as a descriptive parameter of its overall length, as it can be measured by optical methods. After solving each particular FCG step, the crack front increment is smoothed and fitted by a 7th degree polynomial to minimize the unavoidable numerical noise associated with the $K_I(z)$ solution. Such high order polynomial was chosen to capture the odd K_I distributions typical of shallow cracks. The simulated edge-cracked plates are built with the same overall dimensions *H*, *B*, and *W*. The initial edge cracks are introduced with idealized straight fronts, but with different depths a_0. Values of Δa_{jmean} between $0.002B$ and $0.05B$ were used along the FCG simulation, to deal with convergence issues in the calculation of the crack front in step $j+1$. The plate models assume symmetric boundary condition at the plate mid-plane $z = 0$ and are supposed tensioned by a unitary uniformly distributed load at their upper and lower boundaries. Table 2 shows the parameters used in the various models.

Table 2: Parameters used to model the edge-cracked plates.

Poisson's ratio	$\nu = 0.3$
Young's modulus	$E = 200$GPa
Plate Thickness	$B = 5$
Plate Width	$W = 4 \cdot B$
Plate Height	$H = 2.5 \cdot B$
Crack initial length	$a_0 = 0.02 \cdot B$, $0.2 \cdot B$, and B
Paris' rule exponent	$n = 2.0$ and 4.0

Figure 5 shows how the 3D to 2D SIF ratio $K_I(z)/K_{I,2D}$ varies along the crack front with increasing values of a_{surf} for $a_0/B = 0.02$ and a Paris' exponent $n = 2$, and the crack front shape evolution along the plate thickness for the same crack growth stages, quantified by the $(a(z) - a_{min})/B$ ratio. The shapes assumed by the crack front while it grows from the initially straight profile with $a_0/B = 0.02$ show first an anti-tunneling and then a tunneling effect, driven by the non-uniform $K_I(z)$ distribution along the crack front at each crack increment. This non-intuitive behavior occurs because the crack front naturally curves itself looking for a more uniform SIF distribution along it. The non-uniform SIF distribution along the initially straight crack front tends to disappear after the crack propagates for a while and gradually assumes its characteristic slight curved front. For other similar results see Góes et al. (2013).

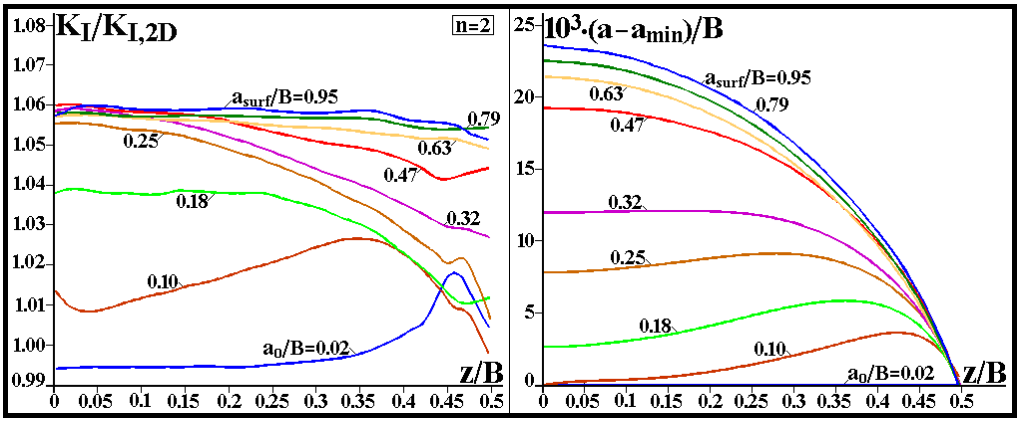

Figure 5: Evolution of the 3D to 2D SIF ratio along the crack front K_I/K_{I2D} and of the crack front shape as the crack grows from an initially straight front, for $a_0/B = 0.02$ and $n = 2$.

Such results deserve some comments. Although to assume that FCG rates are controlled by the crack driving forces is a consensual hypothesis, there is some dispute on which are the actual FCG driving forces. Some prefer ΔK and K_{max} while others defend the use of $\Delta K_{eff} = K_{max} - K_{op}$, but this point is irrelevant for this work. Assuming fixed load conditions, Paris' rule usually fits well the phase II of the FCG curves of many structural alloys. Hence it has been successfully used to model 1-D FCG supposing that the crack growth is controlled by ΔK and uniform along their front in that phase, neglecting that the fatigue damage process may and probably locally vary along their fronts due to microscopic non-homogeneities. Corner and surface 2D cracks can be modeled in the same way, if it is recognized that their SIF values vary along their fronts. Such macroscopic procedures are acceptable if the cracks are large enough because the specimens used to measure FCG properties generate *da/dN* curves that are obtained by fitting the average behavior of their entire crack front. The original results presented in this paper show how such a classical assumption can explain why fatigue cracks like to propagate with a slight curved crack front as a consequence of their attempt to achieve an iso-K_I regime along them. In this sense, such results explain as well why real cracks do not grow by fatigue maintaining a straight front. Hence, albeit it is not possible to simulate what is actually happening at every instant along a real crack front by using the same Paris' constants for every node along the modeled crack front, it certainly can be shown where this (macroscopically reasonable) assumption leads to. In this way, the results obtained here also demonstrate that deeper tunneling effects should be associated with further details not included in this model, like plasticity-induced crack closure, for example. Indeed, if as expected closure effects vary significantly along the crack front inducing non-negligible variations on the ΔK_{eff} values along it, and if ΔK_{eff} is the actual driving force for FCG as assumed by the many supporters of the classical Elberian model, then more pronounced tunneling effects could be expected in such cases. However, such a fascinating argument cannot be further pursued here due to space limitations.

5. CONCLUSIONS

FE analyses were used to simulate 3D effects on stress/strain fields close to notch and crack tips. It was observed that the stress and strain concentration along the notch tips is variable, but the σ_y gradient ahead of it can be obtained from the plane 2D solution, although it causes an out-of-plane restriction on the material that tends to lead the notch tip to plane-strain condition as the tip radius grows sharper ($\rho \rightarrow 0$). Further on, sub-modeling techniques were used to examine 3D effects present in cracks on the edge of tensioned large plates with different thickness-to-crack-length (B/a) ratios. Crack tip LE stress/strain fields were obtained taking into account the full load description, not restricted to *K*-field limitations and long crack assumptions, intrinsically considering *T*-stress and nominal stress effects. SIF were observed to vary along the crack front, presenting maxima K_I values always higher than the 2D solution. The influence of the B/a ratio on the $K_{I,mp}$ was obtained, and describes a smooth transient from the long crack solution presented before in the literature for $B/a = 0.1$) and the plane 2D solution (for $B/a = 100$). It was observed that $K_{I,max}$ is always higher than the 2D predictions. Finally, several FCG were performed, showing that initially straight cracks progressively curved their front during propagation, simultaneously flattening the K_I distribution along the front. After some transient propagation, all cracks converged to the same regime crack propagation front, with tunneling depth close to 2.5% of *B*.

6. ACKNOWLEDGMENTS

CNPq provided scholarships for Castro,JTP and Meggiolaro,MA; Dr. Vasudevan,A from ONR, the Office of Naval Research, US Navy, has contributed with many stimulating discussions; and ONR has partially support this research.

7. REFERENCES

Bazant ZP, Estenssoro LF (1979). Surface singularity and crack propagation. Int J Solids Struct 15:405-426.

Castro JTP; Meggiolaro MA; Miranda ACO; Wu H; Imad A; Nouredine B (2012). Prediction of fatigue crack initiation lives at elongated notch roots using short crack concepts. *Int J Fatigue* 42, 172-182.

Creager M, Paris PC (1967). Elastic field equations for blunt cracks with reference to stress corrosion cracking. Int J Fract 3:247-252.

Góes RCO; Castro JTP; Martha LF (2013). 3D effects around notch and crack tips. *Int J Fatigue*, in press.

Nakamura T, Parks DM (1990). Three-dimensional crack front fields in thin ductile plate. J Mech Phys Sol 38:787-812.

Pilkey W, Pilkey D, Peterson R (2008). Peterson's stress concentration factors. Wiley.

Savin GN (1968). Stress Distribution around Holes. NASA Technical Translation.

Tada H, Paris PC, Irwin GR (2000). The Stress Analysis of Cracks Handbook, 3rd ed. ASM.

Youngdahl CK, Sternberg E (1966). Three-dimensional stress concentration around a cylindrical hole in a semi-infinite elastic body. J App Mech 33:855-865.

Yu P, Guo W, She C, Zhao J (2008). The influence of Poissons ratio on thickness-dependent stress concentration at elliptic holes in elastic plates. Int J Fatigue 30:165-171.

8. RESPONSABILITY NOTICE

The authors are the only responsible for the printed material included in this paper.